JOURNAL OF MATERIALS SCIENCE 9 (1974) 1631-1643

The microstructure of Al–8 wt % Fe-based alloys prepared by rapid quenching from the liquid state

M. H. JACOBS, A. G. DOGGETT, M. J. STOWELL
TI Research Laboratories, Hinxton Hall, Hinxton, Saffron Walden, Essex, UK

The results of a transmission electron microscope study of the microstructure of splat-quenched Al–8% Fe are described in detail. Two distinct structures, zone A and zone B, are examined in as-quenched samples, and each characterized in terms of the dispersions and types of phases present. The decomposition behaviours of zone A and zone B during annealing at temperatures between 573 and 823 K (300 and 550° C) are investigated and the associated phase transformations determined. The effect on the as-quenched, and annealed, microstructures of adding either 3% Mn or 1% Zr to the alloy is described. The observed microstructures and phase transformations are correlated with micro-hardness measurements.

1. Introduction

The "splat-quenching" technique has been used extensively in recent years as a means of solidifying materials at very high cooling rates, in excess of 10^5 K sec^{-1}. The microstructural characteristics of splat-quenched materials have been the subject of a number of investigations (see review by Anantharaman and Suryanarayana [1]). New metastable crystalline phases, new amorphous phases and the retention of supersaturated solid solutions with solute-concentrations far exceeding those obtainable by solid-state quenching have been observed. In addition to their intrinsic interest, from the view-point of theoretical materials science, the results obtained with some alloys have indicated the possibility of exploiting the splat-quenching technique as a means of producing commercially-useful alloys. For example, Grant [2] has splat-quenched several established alloys, including stainless steel and conventional aluminium alloys, and obtained a marked improvement in their mechanical properties.

This paper is concerned with the metastable structures formed in splat-quenched Al–Fe-based alloys, and represents an extension of an earlier study of alloys containing between 4 and 24% Fe* which was carried out by Jones [3]. He found that a transition in the optical microstructure was revealed in as-quenched splats when polished cross-sections were etched in Keller's reagent. The layers adjacent to each surface, which were characterized by a slight response to etching, he designated as zone A. The central region was strongly etched, and this he designated as zone B. He found that the hardness of zone A ($\sim$ 260 kg mm^{-2}) was appreciably higher than that of zone B ($\sim$ 100 kg mm^{-2}). By transmission electron microscopy, he showed that zone A consisted of a fine-scale, second-phase cellular network (cell diameter $\sim$ 30 nm) contained within grains of α–Al, whereas zone B consisted of a much coarser network structure (cell diameter 0.1 to 0.5 μm) also contained within grains of α–Al. X-ray diffractometer measurements on zone A showed asymmetrical broadening and shifting of α–Al reflections, relative to a pure Al standard, corresponding to a reduction in lattice parameter. He interpreted these results as indicating an enhanced solid solubility of Fe in Al, as did Tonejc and Bonefačić [4] in an independent investigation. Jones detected no shift of the α–Al reflections of zone B.

The chief objective of the present study was to provide detailed microstructural information in support of the work of Thursfield and Stowell [5] in which the mechanical and physical

*All compositions are in wt %.

properties, at elevated temperatures, of compacted and extruded Al–Fe base material were evaluated. Transmission electron microscopy was used to study the microstructures of electropolished splats, both in the as-quenched condition and also after subsequent isothermal annealing treatments. Most of the samples were prepared by the "gun" technique of Duwez and Willens [6]. A few reference samples were cut from the bulk material studied by Thursfield and Stowell [5] to ensure equivalence of microstructures (the bulk material was prepared by grinding splatted material, produced by a gas-atomization/spray-quenching technique [7], which was subsequently compacted and extruded into bar stock). The structural characteristics of an Al–8% Fe alloy, reported briefly in an earlier publication [8], are described in detail. These observations are followed by a description of the microstructural changes produced by an addition of 3% manganese or 1% zirconium to this base material.

2. Experimental procedure

The Al–8% Fe alloy was prepared by alloying high-purity Al, Al–4% Fe and Al–11% Fe master alloys supplied by the British Aluminium Co Ltd. The Al–8% Fe–3% Mn alloy was prepared by alloying high purity Al and Mn with the Al–11% Fe master alloy. The Al–8% Fe–1% Zr alloy was prepared by alloying Al–8% Fe with an Al–6% Zr master alloy supplied by the British Aluminium Co Ltd and high purity Fe supplied by BISRA. The impurity levels of all three alloys were low and chemical analysis showed typically 0.1% Si and 0.005% Cu as the major impurities. Samples, 3 mm in diameter and 5 mm long, suitable for melting in the "gun" splat-quenching apparatus, were machined from this bar stock.

The same "gun" that was used by Jones [3] was used in the present work. The samples were melted, and then preheated to a temperature ~1320 K, in a graphite crucible and then expelled by means of an argon shock wave on to a grit-blasted copper substrate at room temperature. The quenched splats were ~ 2 cm in diameter and had a thickness in the range 30 to 100 μm. They were detached from the substrate with a sharp knife.

The heat-treatments were carried out in an air furnace controlled to within ± 5 K of the desired temperature. 3 mm discs for electron microscopy were prepared by a standard electropolishing technique, using an electrolyte of perchloric acid, glycerol and ethyl alcohol in the proportions 1:2:7 by volume. The thin foils were examined in an AEI EM6G electron microscope operating at 100 kV. A few of the foils were examined in a combined electron microscope/microanalyzer (EMMA-3) [9, 10]. The X-ray microanalyses were performed with a 100 kV electron probe, focused to a 100 nm spot at the specimen, and the raw X-ray intensities were converted into mass-concentrations by means of a correction procedure developed specifically for thin foils [11, 12].

3. Microstructure of Al–8% Fe

3.1. As-quenched structures

Before dealing with the microstructures of zone A and zone B in detail, it should be pointed out that a common feature of both zones was the presence of primary intermetallic particles (~ 0.5 μm in diameter) which were distributed throughout the splats. An example of primary particles in zone A is shown in Fig. 1a; similar particles were observed in zone B. The particles were of two types: either the metastable $FeAl_6$ phase [13], as observed by Jones [3], or the equilibrium $FeAl_3$ phase [14]. No preferred site for these particles within zone A or zone B was identified, although they frequently tended to be present as groups rather than being uniformly distributed in the zone.

3.1.1. Structure of zone A

The characteristic network structure of zone A is illustrated in Fig. 1a and b, which were obtained from thin foil sections parallel to the plane of the splat. The structure consisted of α–Al grains, which contained cells of α–Al separated by a network of second-phase material. The α–Al grains were approximately 1 μm in diameter and electron diffraction studies, performed on neighbouring pairs of grains, indicated large orientation changes (usually > 10°) across the grain boundaries. To within the limits detectable by electron diffraction, all the α–Al cells within a grain had the same orientation. Some areas, such as that shown in Fig. 1a, contained many primary particles which had apparently acted as nuclei for the α–Al grains; within these grains the α–Al cells were elongated along radial directions. Primary particles were absent in other areas (see Fig. 1b) and in these regions the α–Al cells were more equiaxed in shape.

The average spacing of the second-phase

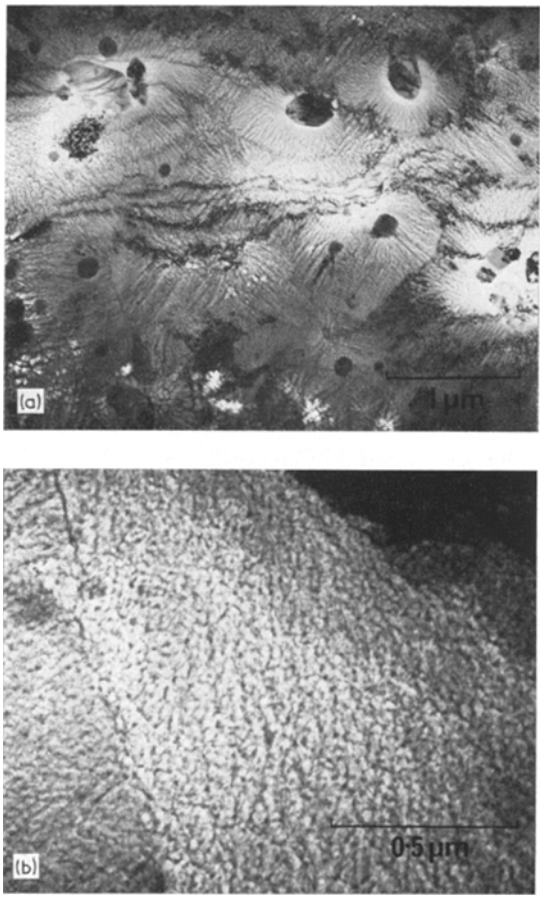

Figure 1 Al–8% Fe, showing structure of as-quenched zone A: (a) primary particles surrounded by elongated network; (b) equiaxed network.

network in zone A was about 30 nm, although large deviations from this value were not uncommon. In regions where the network was very coarse (> 100 nm cell diameter) the structure merged into that characteristic of zone B, which is described in Section 3.1.2.

The characteristic electron diffraction pattern obtained from zone A consisted of a ring pattern superimposed on a spot pattern produced by the α–Al matrix. One half of such a ring pattern is shown in Fig. 2; several of the observed rings were too weak to be reproduced photographically, but all the observed rings are indicated diagrammatically on the right. It is to be noted that ring number 3 was always very much more intense than any of the other rings. Before describing the interpretation of this ring pattern it should be emphasized that no detectable change in the relative intensities of the rings was observed when foils were tilted through angles of up to ± 30° from the horizontal position in the electron microscope. In particular, no tendency towards arcing of the rings was observed and it was concluded that the network phase was not textured. This conclusion was reinforced by an examination of a thin microtomed cross-section of a splat: the ring pattern obtained from zone A was identical to that shown in Fig. 2. Fig. 3 shows a dark-field micrograph obtained from this cross-section by positioning the objective aperture on the most intense ring (number 3 in Fig. 2); small crystallites, about 10 nm in diameter, were highlighted within the intercellular regions. It was concluded that the network of zone A was composed of randomly-oriented, small crystallites. In an earlier publication [8] it was stated that the crystallites were of a body-centred cubic phase, close in composition to FeAl. This identification was obtained from inferior diffraction patterns. More recently, the attainment of better diffraction patterns enabled the *d*-values corresponding to the less intense rings to be determined accurately. The results, which are listed in Table I, were not in accord with the bcc unit cell ascribed earlier. Moreover, good agreement was obtained with the *d*-values calculated for a cubic unit cell with a lattice parameter of 0.360 nm

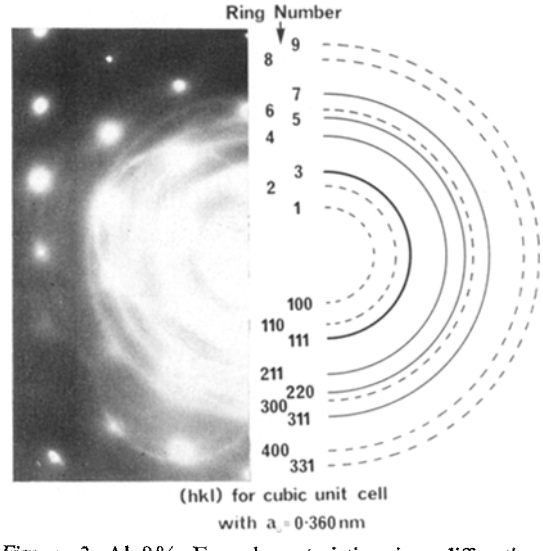

Figure 2 Al–8% Fe: characteristic ring diffraction pattern, and explanatory diagram, from zone A. (Note: the rings centred about the aluminium reflections are due to double diffraction.)

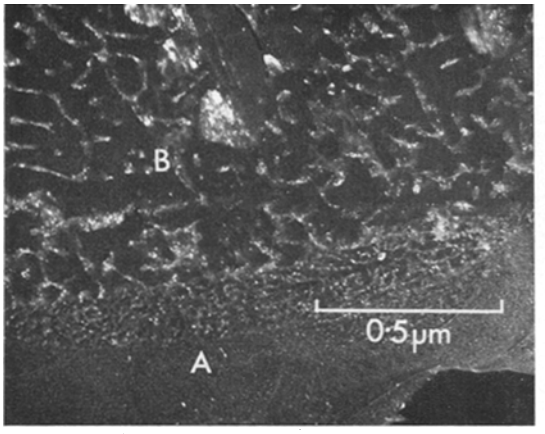

Figure 3 Al–8% Fe: microtomed cross-section of as-quenched splat with zone A and zone B, labelled A and B, respectively. Dark-field micrograph obtained with ring number 3 of Fig. 2, highlighting small crystallites.

TABLE I *d*-values measured from Fig. 2

Ring number	Relative intensity	*d*-value (nm) ± 0.003 nm
1	VW	0.364
2	VW	0.252
3	VS	0.208
4	S	0.147
5	W	0.127
6	VW	0.120
7	W	0.108
8	VW	0.089
9	VW	0.083

VS = very strong; S = strong; W = weak; VW = very weak.

TABLE II *d*-values for a cubic unit cell with $a = 0.360$ nm

hkl	*d*-value (nm)
100	0.360
110	0.254
111	0.208
211	0.147
220	0.127
300,221	0.120
311	0.109
400	0.090
331	0.083

(see Table II). The reflections observed were not those demanded by a simple space group (e.g. bcc, fcc or diamond-cubic) and a more detailed interpretation of the crystal structure was not

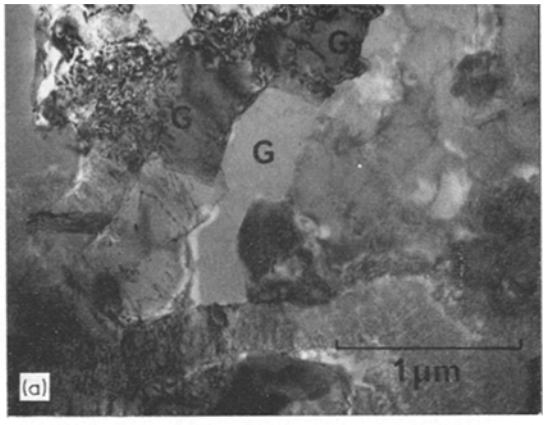

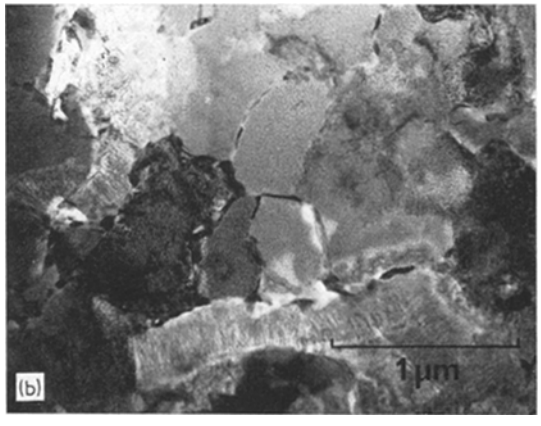

Figure 4 Al–8% Fe: (a) as-quenched zone A region showing grains, G, of complete solid solution; (b) the same area as (a) after annealing for 2 min at 653 K, showing small spheroidal precipitates.

achieved. Nonetheless, it seems highly likely that the unknown phase was iron-rich with, possibly, aluminium atoms as an integral part of the crystal structure.

X-ray diffractometer measurements on splats which, when examined later by electron microscopy, were found to contain a high volume fraction of very fine scale network (< 30 nm spacing) showed stronger α–Al reflections corresponding to material with a reduced lattice parameter [3] than did splats which contained mostly coarse network (30 to 50 nm spacing). This result suggested that the α–Al grains which contained the finer network were more highly supersaturated in iron than those which contained the coarser network, but this point was not proved conclusively. It was, nevertheless, in line with the results obtained from groups of apparently completely supersaturated α–Al

grains, each $\sim$ 0.5 μm diameter, which were sometimes observed. Some examples are labelled G in Fig. 4a; a network structure could not be resolved in these grains in the electron microscope. X-ray microanalysis of these grains in EMMA-3 [12], using a 100 kV electron probe of 100 nm diameter, showed them to contain 8.3 $\pm$ 0.5% Fe, with balance aluminium. Since the maximum equilibrium solid solubility of iron in aluminium is only 0.05% Fe [15], it was concluded that the grains were highly supersaturated. This was substantiated by a subsequent annealing treatment at 653 K for 2 min, during which a high density of zones was precipitated within the grains (Fig. 4b), as described in more detail in Section 3.2.1.

3.1.2. Structure of zone B

The chief characteristic of zone B was that the second phase network was on a much coarser scale than that of zone A. Also, the α–Al grains of zone B tended to be larger in diameter (up to about 5 μm) than those in zone A. A sharp demarcation between zone A and zone B was apparent in the microtomed cross-section (Fig. 3), but the distinction was normally less clear in the electropolished planar sections. The major difficulty which precluded a ready distinction was that much of the coarse network gave rise to a diffraction pattern with rings identical in diameter to those characteristic of zone A. These rings tended to be less diffuse than those produced by zone A, probably because the crystallite size was larger.

The microstructure in some regions of zone B was, however, markedly different from that of zone A. This is illustrated in Fig. 5a. The network was very coarse ($\sim$0.3 μm cell diameter) and consisted predominantly of the equilibrium $FeAl_3$ phase. The network was single-crystal over extensive areas (several cell diameters wide), as is illustrated by the dark-field micrograph, Fig. 5b, which was obtained with a $FeAl_3$ reflection. Similar areas composed of the metastable $FeAl_6$ phase were also observed, but these were less common.

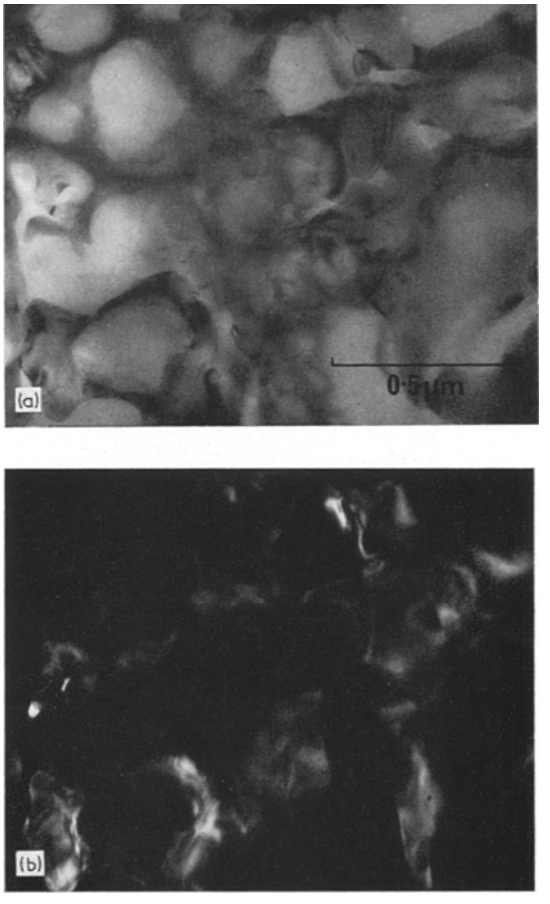

Figure 5 Al–8% Fe: (a) network structure of $FeAl_3$ in as-quenched zone B; (b) dark-field micrograph of (a) obtained with a $FeAl_3$ reflection.

3.2. Microstructural changes during annealing

3.2.1. Decomposition of zone A

Consider first of all the fine-scale network structure which comprised the major portion of the as-quenched microstructure. The only microstructural change observed in samples annealed for up to 3½ h at 573 K was the slow growth of particles at the α–Al grain boundaries (see Fig. 6). These particles were identified, by electron diffraction, as the metastable $FeAl_6$ phase.

More extensive microstructural changes occurred when zone A was annealed at 653 K. After being annealed for 30 min, the network had decomposed in some regions into needle-shaped particles. After 2 h the transformation was complete (Fig. 7a) and the needles were approximately 250 nm in length. This transformation was characterized by the gradual disappearance of the ring pattern, associated with the network structure, which was replaced by a streaked diffraction pattern (an example is shown inset in Fig. 7a). The geometry of the streaks indicated that the needles possessed an

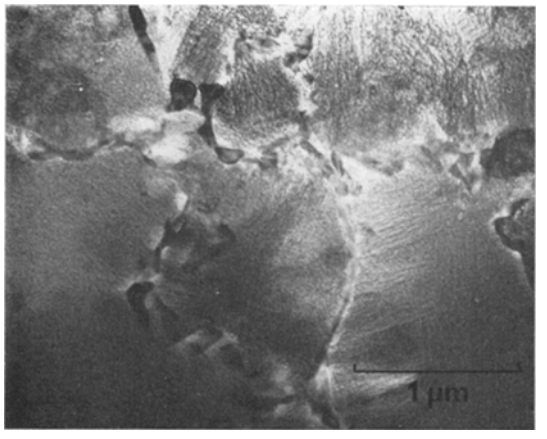

Figure 6 Al–8% Fe: zone A annealed for 3½ h at 573 K. Note the precipitates of $FeAl_6$ at the grain boundaries.

orientation relationship with each α–Al grain, and also that the planar misfit with the matrix along the needle length was very small. The needles coarsened during further annealing and after a total of 4 h at 653 K they were approximately 0.5 μm in length and 25 nm wide (Fig. 7b). These needles were large enough to give rise to a well-defined spot diffraction pattern; an example obtained from an α–Al grain in (001) orientation is shown in Fig. 7c together with an explanatory diagram. The needles were aligned along the ⟨100⟩ directions of the matrix and an analysis of the diffraction pattern (Fig. 7c) showed them to have the monoclinic $FeAl_3$ structure (this identification was confirmed by diffraction patterns containing other sections of the reciprocal lattice). There were two equivalent orientations for needles along each matrix cube direction, e.g. for the needles along [100] α–Al these were:

(i) (010 needle // (100) α–Al
[$\bar{1}$00] needle // [010] α–Al
(ii) (010) needle // (100) α–Al
[100] needle // [001] α–Al.

It is to be noted that the misfit between the $FeAl_3$ needle and the matrix was very small along the needle length, for the *b*-lattice parameter of $FeAl_3$ (0.8083 nm) [14] was very nearly twice the *a*-parameter (0.402 nm) of the α–Al matrix.

The transformation from a network of small, cubic crystallites to oriented needles of $FeAl_3$ occurred more rapidly at 773 K and after 15 min the needles had coarsened into large cuboidal-shaped particles. In a sample annealed for 15 min at 823 K the trend towards spheroidization of the $FeAl_3$ particles was even more marked.

Finally, consider the small single-phase grains that were highly supersaturated with iron in the as-quenched condition. During the first few minutes of annealing at 653 K a high density of spheroidal zones, almost certainly iron-rich and about 10 nm in diameter, was precipitated from the α–Al matrix (Fig. 4b). A careful analysis of those zones, by electron diffraction, showed them to have a cubic unit cell (diamond-cubic, with $a = 0.585 \pm 0.005$ nm) which was oriented with respect to the matrix as follows:

(111) precipitate // (001) matrix
[$\bar{1}$10] precipitate // [010] matrix.

This relationship between the zones and the matrix is illustrated by the stereographic projection shown in Fig. 8a, which was used to interpret the diffraction pattern (Fig. 8b) obtained from a matrix grain in (001) orientation. There are six equivalent orientations for the precipitate (its {111} planes may be parallel to each of the three independent cube planes of the matrix and there are two equivalent orientations in each case). Thus the (111), ($\bar{1}$10) and ($\bar{1}\bar{1}$2) reciprocal lattice sections are superimposed on the matrix (001) section. If all equivalent orientations of the precipitate, and reflections arising from double diffraction, are considered then the pattern shown bottom left of Fig. 8b would be expected. This is in good agreement with the observed pattern when reflections in close proximity are merged together to form a broad region of diffracted intensity. Further support for the proposed unit cell was provided by the diffraction pattern (Fig. 8c) which was obtained from a grain in {111} orientation. According to Fig. 8a, if the zone axis of the matrix is (111) then the diffraction pattern will contain a (202) precipitate reflection which, with respect to the origin, makes an angle of 98° (± 1°) in relation to the ($\bar{2}$20) reflection of the matrix. Likewise, if the zone axis of the matrix is ($\bar{1}\bar{1}$1), the pattern will contain a ($\bar{1}$11) precipitate reflection at 24° (± 1°) from the ($\bar{2}$20) reflection of the matrix. If all equivalent orientations of the precipitate, and reflections arising from double diffraction, are considered then the pattern shown diagrammatically in Fig. 8c would be expected. Indeed, this was in excellent agreement with the observed diffraction pattern.

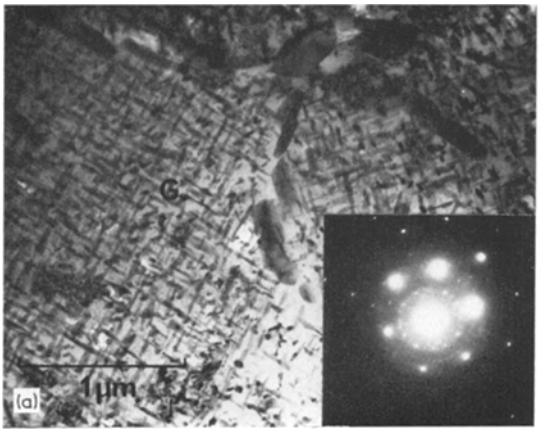

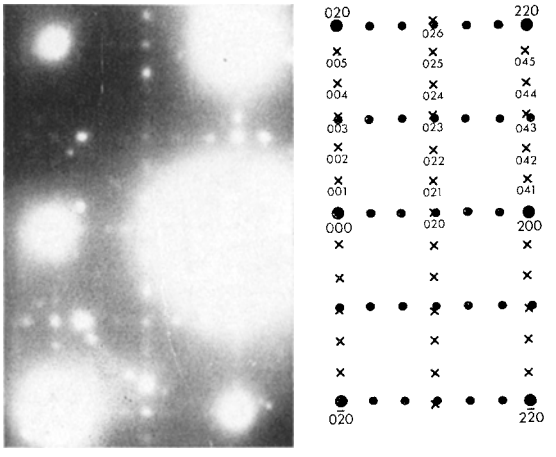

(c)

● α-Al matrix

× $FeAl_3$ needle along [100] α-Al

• $FeAl_3$ needle along [010] α-Al

Figure 7 (a) Al–8% Fe: zone A annealed for 2 h at 653 K. The inset diffraction pattern was obtained from the grain labelled G. (b) Al–8% Fe: zone A annealed for 4 h at 653 K. (c) Diffraction pattern, plus explanatory diagram, obtained from the needles of $FeAl_3$ shown in (b).

The precipitate reflections observed on several other diffraction patterns (notably, the {123} and {012} sections of the matrix) were also in excellent agreement with the proposed orientation relationship and unit cell.

After 15 min at 653 K the zones began to transform into needle-shaped precipitates. At 708 K the decomposition of the solid solution was more rapid and after 5 min most of the zones had transformed into needles, some of which were longer than 0.25 μm and these were identified as the equilibrium $FeAl_3$ phase.

3.2.2. Decomposition of zone B

No change in the coarse network structure of zone B was detected in samples annealed for up to $3\frac{1}{2}$ h at 573 K. At 653 K, the coarse network of cubic crystallites transformed to needles of $FeAl_3$ in a manner similar to zone A. The coarser regions of cellular $FeAl_3$ gradually spheroidized, which resulted in some isolated particles after annealing for 4 h (Fig. 9).

4. Microstructure of Al–8% Fe–3% Mn

The optical microstructures of Al–8% Fe–3% Mn splats in the as-quenched condition were similar to those of Al–8% Fe; zone A and zone B were revealed on a polished cross-section etched with Keller's reagent. Electropolished splats were examined by electron microscopy and the characteristic structures of zone A and zone B were found to be qualitatively similar to those of the binary alloy. Nevertheless, the addition of manganese to the material produced marked changes in the decomposition processes which occurred during annealing. The associated phase changes are compared and contrasted below with those of Al–8% Fe. In this case it is convenient to describe zone B before zone A.

4.1. Decomposition of zone B

In the as-quenched condition the α–Al grains contained a coarse network of particles. In some regions the network was continuous, but in other regions it was discontinuous (Fig. 10) and sometimes an array of rod-like particles was observed. The electron diffraction patterns obtained from these particles showed that they were orthorhombic with lattice parameters in good agreement with those of the intermetallic

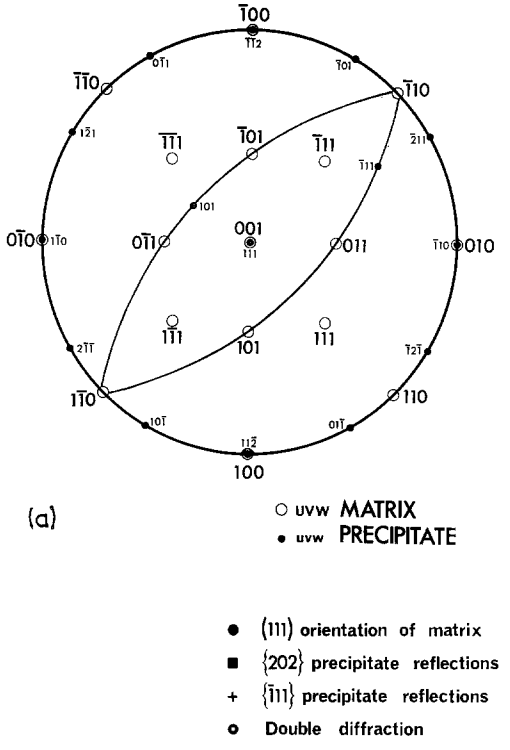

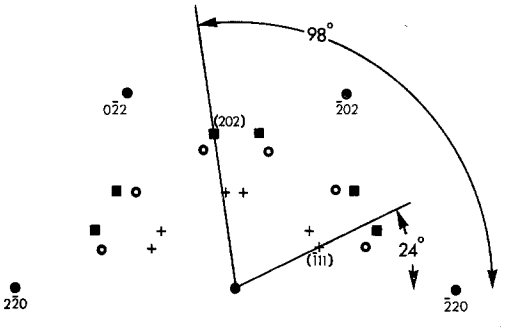

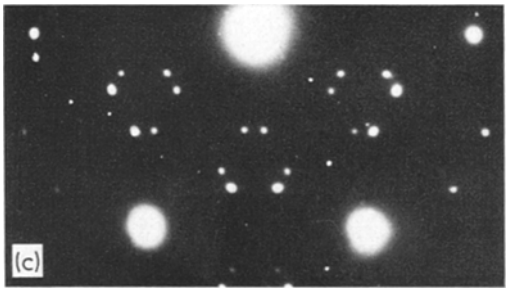

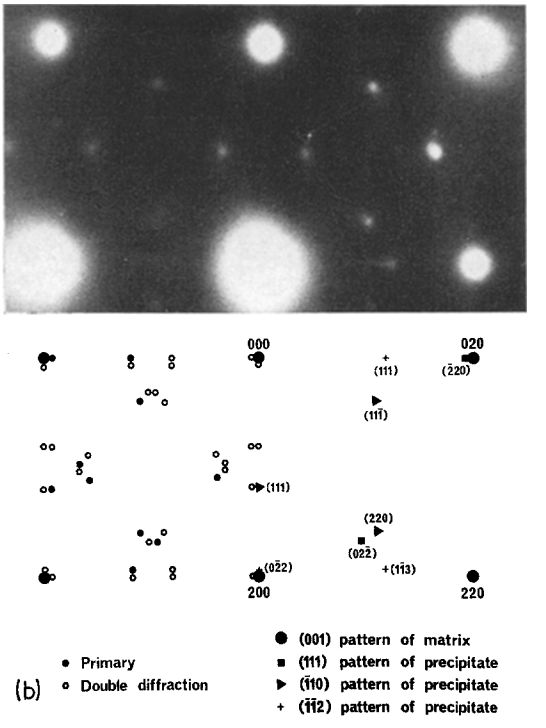

Figure 8 Al–8% Fe: (a) stereographic projection showing the orientation relationship between the diamond-cubic, spheroidal precipitates and the matrix; (b) the diffraction pattern obtained in (001) matrix orientation, plus explanatory diagram; (c) the diffraction pattern obtained in (111) matrix orientation, plus explanatory diagram.

concluded that they could be designated as $(Fe, Mn)Al_6$. This microstructure was not affected appreciably by annealing for $\frac{1}{2}$ h at 823 K. Marked coarsening of the particles was observed in a sample annealed at 923 K for 1 h.

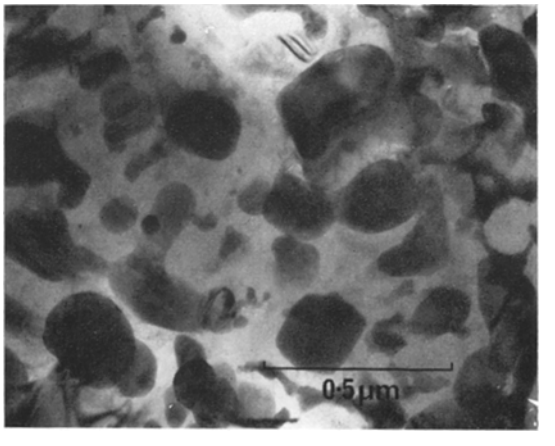

Figure 9 Al–8% Fe: zone B annealed for 4 h at 653 K.

phases $FeAl_6$ and $MnAl_6$, which have closely similar unit cells [13, 16]. Microanalysis of these large particles in EMMA-3 showed that they contained iron and manganese approximately in the weight proportion 3:1. Hence, it was

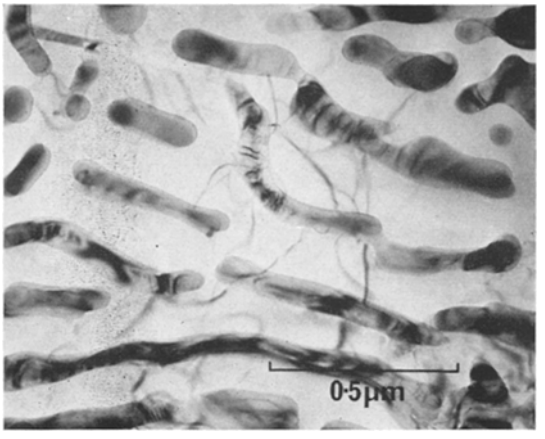

Figure 10 Al–8% Fe–3% Mn: discontinuous network of (Fe, Mn)Al_6 particles in as-quenched zone B.

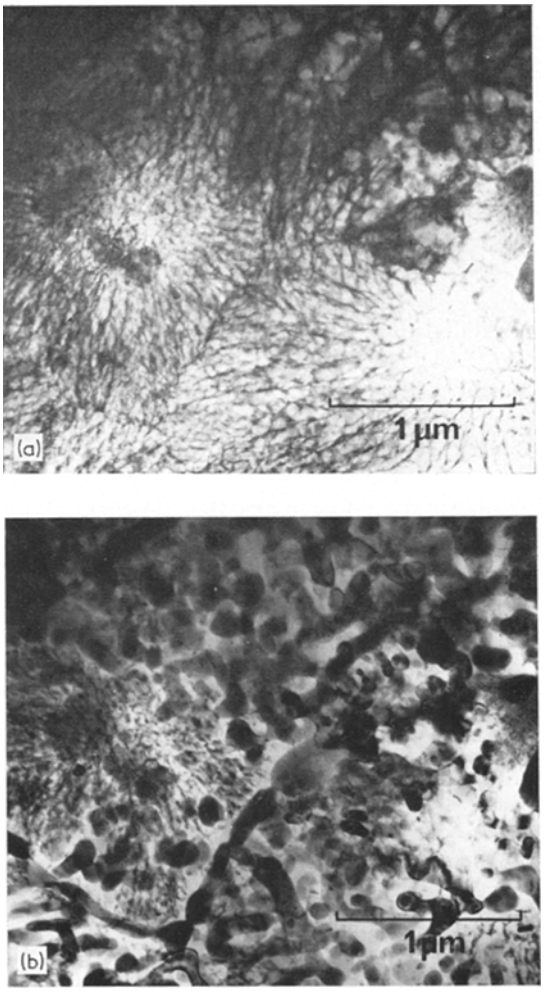

Figure 11 Al–8% Fe–3% Mn: (a) fine-scale network of as-quenched zone A; (b) the same area as (a), after annealing for 2 min at 723 K.

4.2. Decomposition of zone A

The as-quenched microstructure of zone A was similar to that of Al–8% Fe. It was composed of (a) grains of α–Al, about 1 μm diameter, which contained a fine-scale network of second-phase particles, and (b) grains of aluminium, supersaturated with iron and manganese, which were present in a higher volume fraction than their equivalents in the binary alloy.

Fig. 11a illustrates the most common type of network structure with a cell spacing ~ 30 nm. The characteristic ring diffraction pattern generated by this microstructure was identical to that produced by the zone A network of Al–8% Fe (see Fig. 2). The randomly oriented crystallites which comprised the network could be described in terms of the same cubic unit cell as that identified for Al–8% Fe, but it was thought highly likely that manganese atoms were incorporated within the structure in this case. No decomposition of the network was observed in a similar sample when it was annealed for 2 h at 573 K. Fig. 11b shows the same area as Fig. 11a, but after it was annealed for 2 min at 723 K, and illustrates the breakdown of the network to form globular-shaped particles within the grains and at grain boundaries (this same transformation was observed in samples heat-treated prior to electropolishing for electron microscopy). The transformation product was identified as the orthorhombic (Fe, Mn)Al_6 phase, and within the grains these were found to have the following orientation relationship with the matrix:

$$[001]\ (Fe, Mn)Al_6 \,//\, [110]\ \alpha\text{–Al}$$
$$(310)\ (Fe, Mn)Al_6 \,//\, (00\bar{2})\ \alpha\text{–Al}.$$

This relationship is identical to that observed by Adam and Hogan [17] between aluminium and $FeAl_6$ in the Al–$FeAl_6$ eutectic structure of unidirectionally solidified ingots. They concluded that it resulted in low-energy, partially coherent interphase interfaces; because of the close similarity between $FeAl_6$ and (Fe, Mn)Al_6, this would appear to be equally true for the globular particles referred to above. It is to be noted that this transformation was in marked contrast to that of Al–8% Fe, for which the decomposition product was needles of the monoclinic $FeAl_3$ phase.

Consider next the single-phase grains in the as-quenched zone A. Three such grains were microanalyzed in EMMA-3 and were found to contain 9.0 ± 1.0% Fe and 3.5 ± 1.0% Mn, with balance aluminium. Hence, it was concluded that these grains were supersaturated in both iron and manganese (the equilibrium solubilities at 673 K have been reported [15] to be of the order of 0.1% Mn and 0.005% Fe). During annealing at 653 K, these grains decomposed after a few minutes by forming a high density of small spheroidal precipitates, and these had the same diamond-cubic unit cell and orientation relationship with the matrix as their counterpart in the binary alloy. However, it seems almost certain that manganese atoms were incorporated within the precipitates in the ternary alloy. Finally, it should be noted that these spheroids had transformed to globular particles of the (Fe, Mn)Al_6 phase in a sample that was annealed at 653 K for 4 h.

5. Microstructure of Al–8% Fe–1% Zr

The optical microstructures of the Al–8% Fe–1% Zr splats in the as-quenched condition were again similar to those of Al–8% Fe, with zone A and zone B clearly revealed by etching in Keller's reagent. Likewise, the electron microstructures of zone A and zone B were qualitatively similar to those of the binary alloy, but the zone A regions of the ternary alloy tended to have a slightly smaller grain size (0.5 to 1.0 μm) and there was a larger volume fraction of the very fine network (< 30 nm cell diameter) of crystallites with the cubic unit cell.

Samples which were annealed at 653 K for up to 4 h underwent the same transformations as the binary alloy, which may be summarized as follows:

(i) Small spheroidal particles, with the same cubic unit cell as those in the binary alloy, were precipitated from the single-phase grains of solid solution (X-ray microanalysis in EMMA-3 of these grains in the as-quenched condition showed them to contain approximately 8% Fe and 1% Zr).

(ii) The zone A network of crystallites transformed to needles of $FeAl_3$.

(iii) The coarse zone B network of $FeAl_3$ began to spheroidize.

All of these transformations appeared to be unaffected by the presence of zirconium in the alloy.

Some important microstructural observations were obtained from a sample of extruded bar which had been annealed at 573 K for 100 h. In some regions the microstructure consisted of needle-shaped particles of $FeAl_3$ in an aluminium matrix, but in other regions (e.g. that labelled P in Fig. 12) the $FeAl_3$ particles were more globular and were probably derived from the as-quenched zone B structure. Microanalysis with EMMA-3 of several of the particles illustrated in Fig. 12 showed that they contained iron, but no zirconium was detected. In marked contrast, approximately 1% zirconium was detected in the aluminium matrix in between the particles, with only a trace of iron. In the region shown in Fig. 12, all the zirconium appeared to be in solution in the aluminium matrix. However, precipitates of $ZrAl_3$ were identified in other regions of this specimen, and also in a sample annealed for 100 h at 673 K. Three distinct morphologies of the metastable, cubic $ZrAl_3$ precipitates were observed, similar to those described by Ryum [18] and Nes [19] in dilute alloys of zirconium in aluminium:

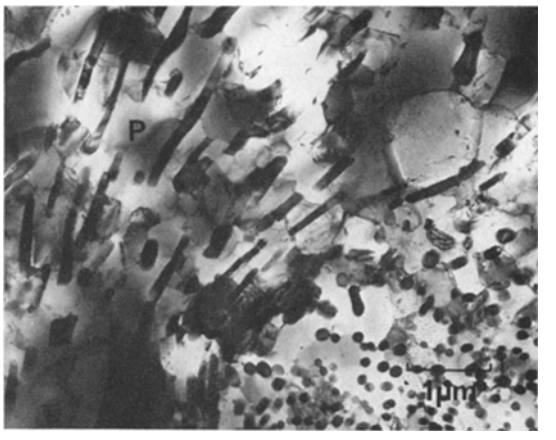

Figure 12 Al–8% Fe–1% Zr: structure of extruded sample after annealing at 573 K for 100 h. The particles labelled P were identified as the $FeAl_3$ phase.

(i) Spheroidal, coherent precipitates, ~ 5 nm in diameter. These are illustrated by Fig. 13a, which was a dark-field micrograph obtained with the precipitate reflection indicated by the arrow in the inset diffraction pattern. The aluminium matrix was in {1 1 1} orientation, and the inner-most hexagonal array of precipitate spots on the diffraction pattern were indexed as {1 1 0} reflections for the metastable, cubic $ZrAl_3$ phase [18].

(ii) Larger precipitates of $ZrAl_3$, sometimes

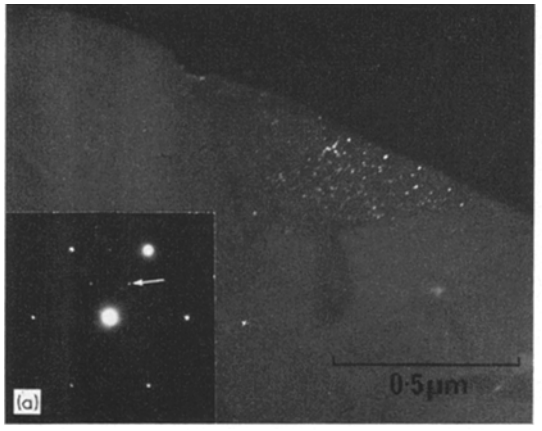

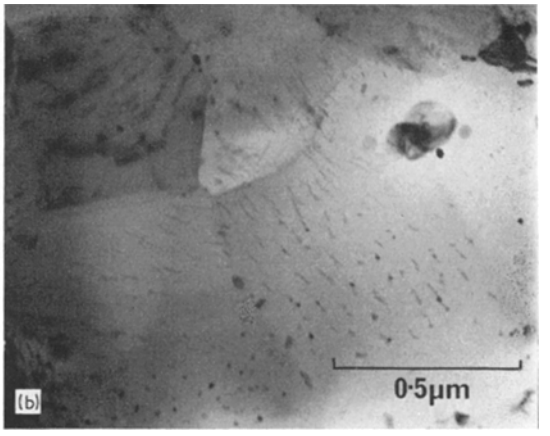

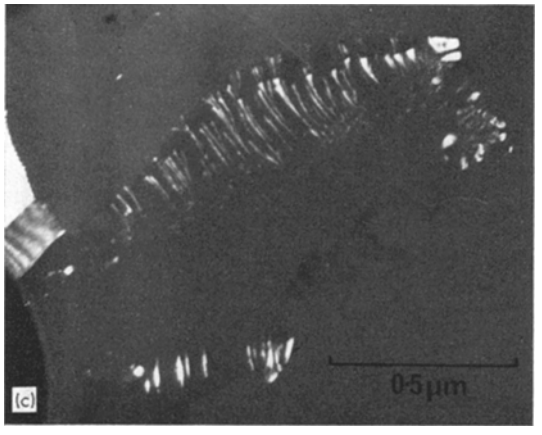

Figure 13 Al–8% Fe–1% Zr: three morphologies of the metastable, cubic $ZrAl_3$ phase. (a) Spheroidal, coherent precipitates in a sample annealed at 673 K for 100 h (dark-field on reflection indicated by the arrow in the inset diffraction pattern). (b) Larger particles. (c) A fan-shaped array (dark-field on a $ZrAl_3$ reflection), in a sample annealed at 573 K for 100 h.

present as rows of particles in the matrix, and sometimes present as particles at grain boundaries (see Fig. 13b).

(iii) Fan-shaped arrays of $ZrAl_3$ precipitates emanating from grain boundaries (Fig. 13c).

In summary, for short annealing times (a few hours) at temperatures between 573 K and 673 K the Al–8% Fe–1% Zr splats decomposed by mechanisms identical to those characteristic of Al–8% Fe. During these short annealing treatments, it seems highly likely that the zirconium was all retained in solution in the aluminium matrix and played no part in the transformations involving the iron-aluminium phases. For long annealing times ($\sim$ 100 h) at 573 to 673 K, the zirconium precipitated from the matrix and formed the three distinct morphologies of the metastable, cubic $ZrAl_3$ phase described above.

6. Discussion

6.1. Relation between microstructure and hardness

The chief objective of this study was to provide detailed microstructural information in support of the work of Thursfield and Stowell [5] in which the mechanical and physical properties of heat-treated, Al–8% Fe-based alloys were evaluated. In the present discussion it is convenient to choose microhardness, measured at room temperature, as the parameter by which the response of the material to annealing treatments is judged.

The microstructural studies showed that only minor changes in the structure of zone B occurred as a result of annealing between 573 and 673 K for a few hours. This is consistent with the results obtained by Jones [3], and confirmed by Thursfield and Stowell [5], that the microhardness of zone B in Al–8% Fe decreased only slightly. In marked contrast, appreciable microstructural changes occurred when zone A regions were annealed for 1 h between 573 and 673 K. These changes are reflected in the microhardness curves, shown in Fig. 14, which were obtained by Thursfield and Stowell. The relation between microstructure and hardness, for each alloy studied, is discussed below.

6.1.1. Al–8% Fe

The reduction in zone A hardness at temperatures above 573 K can be directly correlated with the

decomposition of the crystallites, forming the fine-scale network structure, to needles of the equilibrium $FeAl_3$ phase. A high density of small needles was created during the early stage of the transformation, and these helped to retain some dispersion-hardening of the aluminium matrix. However, at 653 K and higher temperatures, the needles coarsened rapidly into large, spheroidal particles of $FeAl_3$ and this resulted in a rapid decrease in the hardness.

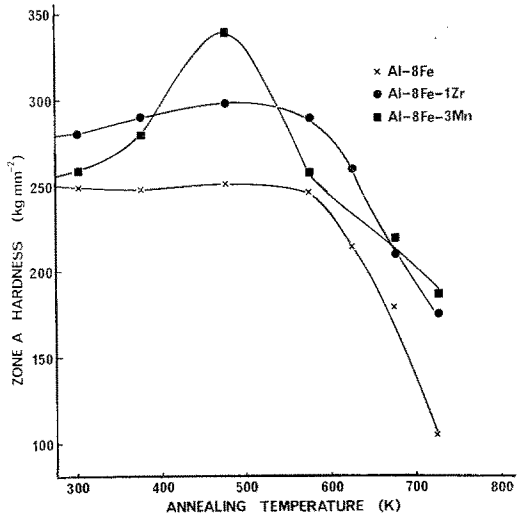

Figure 14 The variation of microhardness (determined at room temperature) of zone A with annealing temperature for Al–8% Fe, and the alloys with 3% Mn or 1% Zr additions, after annealing for 1 h at each temperature (after Thursfield and Stowell [5]).

6.1.2. Al–8% Fe–3% Mn

In the as-quenched condition, the zone A regions contained a much larger volume fraction of grains of complete solid solution, when compared with the binary alloy. The increase in zone A hardness between 200 and 573 K (see Fig. 14) can be attributed to the precipitation of small, spheroidal precipitates from this solid solution. Above 573 K, the fine network of crystallites decomposed to globular particles of $(Fe, Mn)Al_6$, which resulted in an appreciable decrease in the hardness.

6.1.3. Al–8% Fe–1% Zr

It is believed that the higher as-quenched zone A hardness of this alloy, relative to the binary alloy can be directly attributed to two factors: (a) the addition of zirconium refined the grain size of the matrix, and also refined the average network spacing; and (b), the evidence suggests that all the zirconium addition was in solid solution with the aluminium matrix, thereby conferring added strength by solid solution hardening. In samples annealed above 573 K, the iron-aluminium phases decomposed in manners similar to those in the binary alloy. However, in these samples, the zirconium precipitated from the solid solution very slowly as a fine dispersion of the metastable $ZrAl_3$ phase, and this process tended to off-set the loss in dispersion hardening caused by the coarsening of the iron-containing phases and therefore this represents the main reason for the improved mechanical properties of this alloy at temperatures $\sim$ 600 K and above.

6.2. Metastable phases

The unit cells of two new metastable phases are determined in this investigation. The most important metastable phase, from the view-point of its effect on the mechanical properties, was that which constituted the crystallites in the network of zone A. This interdendritic phase was found, by electron diffraction, to have a cubic unit cell with a lattice parameter of 0.360 ± 0.003 nm. Despite the fact that this lattice parameter is in good agreement with that of γ-iron ($a = 0.359$ nm), it must be emphasized that the observed reflections were not those demanded by a fcc structure, or those for any other common cubic structure (e.g. bcc or diamond-cubic) – see Table II. Nevertheless, it seems highly likely that this phase was rich in iron atoms, but neither the composition nor the space group was determined. In the case of the Al–8% Fe–3% Mn alloy, it is probable that manganese atoms partly replaced the iron atoms within the crystallites, which otherwise gave rise to an identical ring diffraction pattern; however, in the Al–8% Fe–1% Zr alloy, the evidence suggests that all the zirconium was retained in solution in the aluminium matrix. It is noteworthy that Blank [20] observed an interdendritic phase in splat-quenched Al–Fe (1 to 4% Fe) which he interpreted as γ-iron: the rings of the (200) and (400) reflections were absent and he attributed this to a fibre texture. This interpretation is not adequate to explain our observations with Al–8% Fe, for not only was a weak (400) reflection observed but also (100), (110), (211) and (300) reflections which are not allowed for the fcc space group. It should be added that the d-values corresponding to these reflections could not be

attributed to either α–Al_2O_3 or γ-Al_2O_3; also, they were significantly different from the d-values associated with the spheroidal particles, discussed below, which were precipitated from the regions of solid solution.

The other metastable phase which was identified was precipitated from the grains of supersaturated solid solution, common to all three alloys studied. The small precipitates (diamond-cubic, with $a = 0.585 \pm 0.005$ nm) were somewhat similar to conventional G.P. zones, but were not completely coherent with the matrix: each precipitate had a small misfit with the matrix along one $\langle 100 \rangle$-direction of the matrix, but in other directions the misfit was large. Since there were found to be six equivalent orientations for these zones, the associated electron diffraction patterns were very complex. The interpretation was made difficult by the fact that in some matrix orientations (e.g. $\{100\}$) the patterns contained broad spots of diffracted intensity, each composed of several independent precipitate reflections in close proximity. It is noteworthy that Blank [20], and Furrer and Warlimont [21] observed similar metastable zones in annealed Al–Fe samples, but the structure of the zones was not determined. Our observations showed that these metastable zones eventually transform to the equilibrium $FeAl_3$ phase. Whether or not the zones may be regarded as a metastable form of $FeAl_3$ could not be ascertained because their chemical composition was not determined.

Finally, the reason why the metastable $FeAl_6$ phase forms at grain boundaries of annealed zone A in Al–8 % Fe, rather than the equilibrium $FeAl_3$ phase, was not determined. Two possibilities, suggested by Jones [22], are that the interfacial kinetics favour the nucleation of $FeAl_6$, or that non-equilibrium segregation to grain boundaries is sufficient to nucleate $FeAl_6$ but not $FeAl_3$.

Acknowledgement

We acknowledge helpful discussions with our colleague, Dr G. Thursfield, who collaborated in this study. This paper is published by permission of the Chairman of Tube Investments Ltd.

References

1. T. R. ANANTHARAMAN and C. SURYANARAYANA, *J. Mater. Sci.* **6** (1971) 1111.
2. N. J. GRANT, *Fizika* **2** (Suppl. 2) 16 Proceedings of the International Conference on Metastable Metallic Alloys, Brela, Yugoslavia, 1970.
3. H. JONES, *Mater. Sci. Eng.* **5** (1969/70) 1.
4. A. TONEJC and A. BONEFAČIĆ, *J. Appl. Phys.* **40** (1969) 419.
5. G. THURSFIELD and M. J. STOWELL, *J. Mater. Sci.* **9** (1974) 1644.
6. P. DUWEZ and R. H. WILLENS, *Trans. Met. Soc. AIME* **227** (1963) 362.
7. G. THURSFIELD and H. JONES, *J. Phys. E: Sci. Instrum.* **4** (1971) 675.
8. M. H. JACOBS, A. G. DOGGETT and M. J. STOWELL, *Fizika* **2** (Suppl. 2) 18. Proceedings of the International Conference on Metastable Metallic Alloys Brela, Yugoslavia, 1970.
9. C. J. COOKE and I. K. OPENSHAW, Proceedings of the 4th National Conference on Electron Probe Analysis, Pasadena, (1969) Paper No. 64, Electron Probe Analysis Society of America, USA.
10. M. H. JACOBS, "Proceedings of the 25th Anniversary Meeting of EMAG", (Institute of Physics, London and Bristol, 1971) p. 138.
11. M. H. JACOBS and MRS. J. BABOROVSKA, "Proceedings of the Fifth European Congress on Electron Microscopy" (Institute of Physics, London and Bristol 1970) p. 136.
12. M. H. JACOBS, *J. Microscopy* **99** (1973) 165.
13. L. K. WALFORD, *Acta Cryst.* **18** (1965) 287.
14. P. J. BLACK, *ibid* **8** (1955) 43, 175.
15. "Equilibrium Diagrams of Aluminium Alloy Systems" (The Aluminium Development Association, London, 1961).
16. L. BÄCKERUD, *Jernkont. Ann.* **152** (1968) 109.
17. C. MCL. ADAM and L. M. HOGAN, *J. Aust. Inst. Met.* **17** (1972) 81.
18. N. RYUM, *Acta Met.* **17** (1969) 269.
19. E. NES, *ibid* **20** (1972) 499.
20. E. BLANK, *Z. Metallk.* **63** (1972) 315, 324.
21. P. FURRER and H. WARLIMONT, *ibid* **64** (1973) 236.
22. H. JONES, *Rep. Progr. Phys.* **36** (1973) 1425.

Received 25 March and accepted 23 April 1974.